A novel algorithm for shape parameter selection in radial basis functions collocation method

(Article begins on next page)

20 May 2024

# A novel algorithm for shape parameter selection in radial basis functions collocation method

M. Gherlone, L. Iurlaro *, M. Di Sciuva
Department of Aerospace Engineering, Politecnico di Torino, Corso Duca degli Abruzzi, 24 10129 Torino, Italy

ABSTRACT

Many Radial Basis Functions (RBFs) contain a free shape parameter that plays an important role for the application of Meshless method to the analysis of multilayered composite and sandwich plates. In most papers the authors end up choosing this shape parameter by trial and error or some other ad hoc means. In this paper a novel algorithm for shape parameter selection, based on a convergence analysis, is pre-sented. The effectiveness of this algorithm is assessed by static analyses of laminated composite and sandwich plates.

## 1. Introduction

The finite element method has been used with great success in many fields (static/dynamic, linear/nonlinear analysis of solids, structures as well as fluid flows) with both academic and industrial applications. Most practical engineering problems related to solids and structures are currently solved using well-known FEM packages that are commercially available. However, the following limitations of displacement-based FEM are becoming increasingly evident: the analyst spends the majority of his time in creating the mesh and this becomes a major component of the simulation cost; stresses are discontinuous and less accurate than displace-ments; when handling large deformation, considerable accuracy is lost because of the element distortion; it is very difficult to sim-ulate crack growth with arbitrary and complex paths due to dis-continuities that do not coincide with the original nodal lines. These are only some of the limitations, but they are sufficient to re-veal the root of the problem: the need to use elements or, in other words, the need to use a mesh. Thus, starting from this observa-tion, the Meshless methods have been proposed.

In fact, Meshless methods [1,2] establish a system of algebraic equations for the whole problem domain without the use of a mesh. Nodes arbitrarily scattered within the problem domain as well as on its boundaries are adopted. These nodes do not form a mesh and do not discretize the problem domain but represent it. Since the distribution of the nodes could be obtained through an automatic process, Meshless methods allow saving the time spent by analysts for mesh creation.

Meshless methods can be grouped into two categories: in the first, methods which establish the algebraic system of equations using the weak form of the problem are collected; methods that use the strong form of the problem belong to the second group.

Due to the use of the weak form, the methods belonging to the first category are not truly Meshless because they require the inte-gration of the equations and, thus, the construction of a computa-tional grid. On the contrary, this is not necessary for the methods of the second category and for this reason they are considered truly Meshless. In these methods, also called Meshless Collocation meth-ods, the strong-form of the governing equations and boundary conditions are directly discretized at the field nodes using simple collocation technique to obtain a set of discretized system equa-tions. The reader is referred to Refs. [1,2] for a detailed description.

In order to investigate the accuracy of a Meshless method belonging to the second category, this paper focus on the static analysis of laminated composite and sandwich plates by means of an unsymmetric Radial Basis Functions collocation method (RBFs). Among all the interpolation schemes, the RBF outperformed all the other methods in terms of accuracy, stability, efficiency and simplicity of implementation. As stated in [3], the system of algebraic equations obtained with the unsymmetric method is in general easier to implement but computationally more expensive than the one obtained with the symmetric method.

There are different types of radial basis functions [3] but among these, the Hardy's multiquadratics (MQ) were ranked the best in accuracy and convergence. However, despite MQ's excellent per-formance, it contains an user defined shape parameter, $c$, which affects the stability and accuracy of the solution. So far, the choice of the optimal value of the shape parameter remains an open

* Corresponding author.
*E-mail addresses:* marco.gherlone@polito.it (M. Gherlone), luigi.iurlaro@polito.it (L. Iurlaro), marco.disciuva@polito.it (M. Di Sciuva).
[1] http://www.polito.it, http://www.aesdo.polito.it.

roblem; no mathematical theory has been developed yet to determine its optimal value. For this purpose, different models are available [4] and will be briefly discussed in Section 2.1.

In this paper, we suggest an alternative method for estimating the optimal shape parameter that is based on a convergence analysis. In order to validate the accuracy of the proposed algorithm, numerical results are presented and compared with the ones available in the open literature. In particular, multilayered composite and sandwich plates subjected to various loads and with different boundary conditions are analyzed using the First-order Shear Deformation Theory and the unsymmetric Radial Basis Functions collocation method with different choices of the optimal shape parameter.

## 2. The unsymmetric radial basis functions collocation method

In this paper the Kansa's unsymmetric collocation method [5] will be adopted. Consider a boundary value problem defined by

$$Du(\boldsymbol{x}) = s(\boldsymbol{x}) \quad \text{on } \Omega \tag{1}$$
$$Bu(\boldsymbol{x}) = f(\boldsymbol{x}) \quad \text{on } \partial\Omega \tag{2}$$

where $\Omega$ is the problem domain, $\partial\Omega$ its boundary, and the operators $D$ and $B$ are linear partial differential operators on $\Omega$ and on $\partial\Omega$, respectively. Points in the interior of the domain are denoted by $(\boldsymbol{x_i}, \ i = 1, \ldots, N_I)$ while those on the boundary are $(\boldsymbol{x_i}, \ i = N_I + 1, \ldots, N_I + N_B = N)$.

The solution $u(\boldsymbol{x})$ may be approximated by using the following RBF-based interpolation

$$\bar{u}(\boldsymbol{x}) = \sum_{i=1}^{N} a_i \phi_i(\|\boldsymbol{x} - \boldsymbol{x_i}\|, c) \tag{3}$$

where $\phi_i$ is the Radial Basis Function (RBF) centered at $\boldsymbol{x_i}$ [5]. The RBF considered is this paper is the multiquadratics (MQ) one, which assumes the following expression

$$\phi_i(\boldsymbol{x}) = (\|\boldsymbol{x} - \boldsymbol{x_i}\|^2 + c^2)^{1/2} \tag{4}$$

where $\|\boldsymbol{x} - \boldsymbol{x_i}\|$ is the Euclidian norm while $c$ is a user-defined shape parameter.

Collocation with the boundary data at the boundary points and with field equations at the interior points leads to

$$\sum_{i=1}^{N} a_i D\phi_i(\|\boldsymbol{x_j} - \boldsymbol{x_i}\|, c) = \Phi(\boldsymbol{x_j}), \quad j = 1, \ldots, N_I \tag{5}$$

$$\sum_{i=1}^{N} a_i B\phi_i(\boldsymbol{x_j} - \boldsymbol{x_i}\|, c) = \lambda(\boldsymbol{x_j}), \quad j = N_I + 1, \ldots, N_I + N_B \tag{6}$$

where $\lambda(\boldsymbol{x_j})$ and $\Phi(\boldsymbol{x_j})$ are the prescribed values at the boundary nodes and the function values at the interior nodes, respectively. In matrix compact form, Eqs. (5) and (6) read

$$[L]\{a\} \equiv \begin{bmatrix} D\phi \\ B\phi \end{bmatrix} \quad \{a\} = \begin{bmatrix} \Phi \\ \lambda \end{bmatrix} \tag{7}$$

with an unsymmetric coefficient matrix $[L]$. The solution of the system (7) gives the unknown vector $\{a\}$.

### 2.1. Methods for shape parameter selection

The accuracy and the well-conditioning of the solution of Eq. (7) depends on $c$. In a number of numerical methods that uses global shape functions, such as the MQ collocation, it has been observed [6] that, as the basis functions become flatter and flatter, the accuracy of the solution improves. This may be obtained increasing the value of $c$, since $\phi_i$ would become, in the limit, a constant function of $x$ (see Eq. (4)). On the other hand, increasing the value of $c$

also leads to a growth of the condition number of the solution matrix which makes the problem ill-conditioned [6]. Ultimately, though, the round off error dominates and the matrix solution becomes unstable; at that point, the solution breaks down.

Table 1 summarizes some of the methods proposed in the literature for the shape parameter calculation: $d$ represents the average distance between nodes, $D$ is the diameter of the minimal circle enclosing all data points, while $N$ is the number of nodes.

The models quoted in Table 1 are related with the number of nodes in the grid and with the distance between them. Among all the approaches collected in Table 1, the Fasshauer 'one is the best in terms of accuracy and has been used both for static and free vibration analyses. In particular, accurate results have been achieved by Ferreira when natural frequencies of composite shells

**Table 1**
Shape parameter selection methods.

| Reference | Shape parameter, $c$ |
|---|---|
| Hardy [7] | $c = 0.815d$ |
| Franke [8] | $c = 1.25D/\sqrt{N}$ |
| Fasshauer [9] | $c = 2/\sqrt{N}$ |
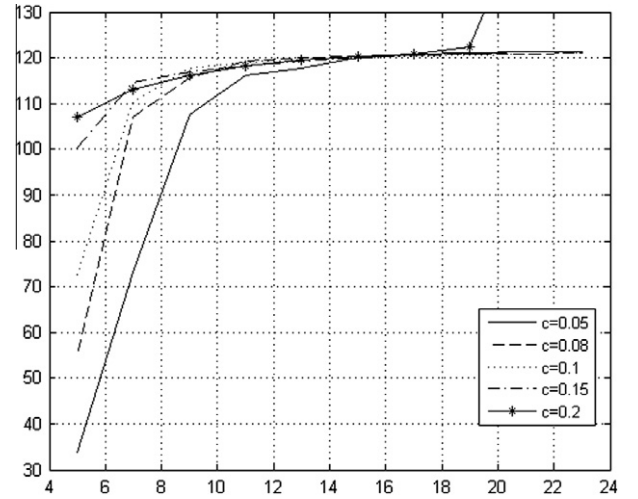


**Fig. 1.** Convergence analysis.
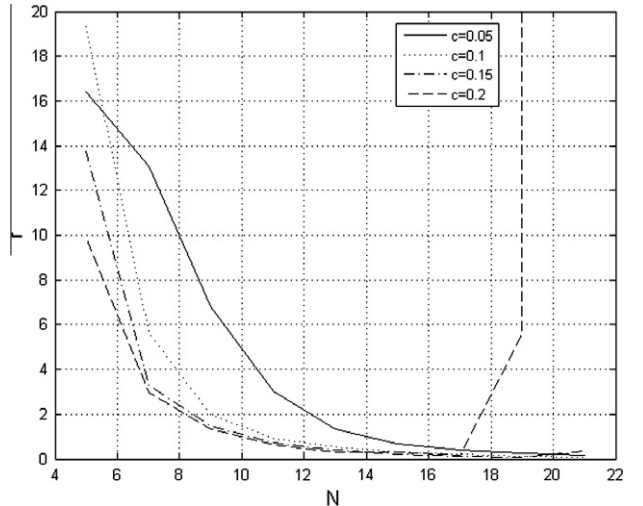


**Fig. 2.** Rate of convergence.

**Table 2**
Mechanical properties of unidirectional lamina.

| $E_L$ | $G_{LT}$ | $v_{LT}$ | $G_{TT}$ |
|---|---|---|---|
| $25 \cdot E_T$ | $0.5 \cdot E_T$ | 0.25 | $0.2 \cdot E_T$ |

are computed by means of multiquadratics radial basis functions [10]. When the radial basis functions are used coupled with the Pseudospectral Method (PS), the estimation of an optimal value of the shape parameter requires a careful selection since the problem could become very ill – conditioned. In [11] Ferreira and Fasshauer suggest a formula a formula for the estimation of the optimal $c$ that depends on the number of nodes. However, according to Rippa [12], the shape parameter should depend on many others factors, such as: distribution of grid points, condition number of the matrix, computer precision and interpolation function, $\phi$.

Building on these observations, Rippa [12] proposed an algorithm allowing to select an optimal value of the shape parameter. This algorithm minimizes a cost function that imitates the behavior of the RMS error between the numerical solution and the exact one. According to [12], the cost function is given by the norm of an error vector $E(c)$ with components

$$E_i(c) = \frac{a_i}{L_{ii}^{-1}} \qquad (8)$$

where $a_i$ is the $i$th component of the vector $\{a\}$ and $L_{ii}^{-1}$ is the $i$th diagonal element of the inverse of the coefficient matrix (Eq.(7)). Thus, the optimal value of the shape parameter is considered as the one which minimizes the cost function $E(c)$. Particular atten-tion must be paid to the interval inside which searching for the optimal $c$; in [4] it is suggested to inspect the cost function on a large interval and then select a smaller one; this procedure is very expensive.

In recent years, the use of radial basis functions coupled with Pseudospectral Method has undergone intensive research since it ensures several potential advantages [11]. Since the original work of Rippa concerns interpolation problems, a modification of his

algorithm is required if it has to be used for the selection of an optimal $c$ in the RBF-PS method. In [13] a modification of the original procedure is suggested.

In this paper we suggest an alternative algorithm for the estimation of the shape parameter based on a convergence analysis.

### 2.2. A novel algorithm for the choice of the shape parameter

The algorithm proposed in this paper estimates the optimal value of the shape parameter $c$ through a convergence analysis, varying the number of nodes $N$ and the shape parameter value itself in a user-defined range. The control variable for the conver-gence analysis in static problems may be chosen as the displace-ment $\bar{w}$ (for example, the normalized maximum displacement of a plate subjected to a pressure load). Fixed the value of the shape parameter in the user-defined range, the solution will be estimated for all the number of nodes in the interval (Fig. 1). As it is possible to understand looking at Fig. 1, solutions with a higher value of the shape parameter reach a value of the control variable greater than those with a lower shape parameter. This behavior is true in the first part of the Fig. 1; when the number of nodes increases, a greater value of $c$ does not ensure a higher value of the control variable. Thus it is not correct to choose a good value of the shape parameter selecting the $c$ that guarantees the fastest convergence for a small number of nodes.

In order to estimate the good value for the shape parameter, the optimization is made on the rate of convergence, defined as follows

$$r(N_j, c_k) = \frac{|\bar{w}(N_{j+1}, c_k) - \bar{w}(N_j, c_k)|}{N_{j+1} - N_j} \qquad (9)$$

where $\bar{w}(N_j, c_k)$ is the solution estimated with $N_j$ nodes and a value of the shape parameter $c_k$.

Chosen a number of nodes $N^*$, the optimal shape parameter is that which ensure the minimum value of $r$. In Fig. 2 the rate of convergence related to the problem of Fig. 1 is represented.

Following this approach, the optimal value of the shape parameter changes with the number of nodes and also, as it will be seen in Section 4, it depends on the regularity of the grid.

**Table 3**
Results for a simply supported laminated composite square plate subjected to sinusoidal pressure.

| $a/h$ | Method | $\bar{w}$ | $\bar{\sigma}_{xx}$ | $\bar{\sigma}_{yy}$ | $\bar{\tau}_{xz}$ | $c_{opt}$ |
|---|---|---|---|---|---|---|
| 4 | FSDT exact | 1.7100 | 0.4059 | 0.5765 | 0.2686 | |
| | Present | 1.7086 | 0.4064 | 0.5773 | 0.2644 | 0.1250 |
| | Fasshauer | 1.7093 | 0.4071 | 0.5779 | 0.2621 | 0.1168 |
| | Franke | 1.7179 | 0.3580 | 0.5912 | 0.5113 | 0.0620 |
| | Hardy | 1.7232 | 0.4013 | 0.5914 | 0.0836 | 0.0584 |
| | Rippa | 1.7099 | 0.4052 | 0.5770 | 0.2572 | 0.1551 |
| 10 | FSDT exact | 0.6628 | 0.4989 | 0.3615 | 0.3181 | |
| | Present | 0.6623 | 0.4986 | 0.3612 | 0.3056 | 0.1600 |
| | Fasshauer | 0.6651 | 0.5021 | 0.3628 | 0.3215 | 0.1168 |
| | Franke | 0.6765 | 0.5465 | 0.3688 | 1.6316 | 0.0620 |
| | Hardy | 0.6812 | 0.5310 | 0.3712 | 0.8263 | 0.0584 |
| | Rippa | 0.6620 | 0.4983 | 0.3611 | 0.3046 | 0.1699 |
| 20 | FSDT exact | 0.4912 | 0.5273 | 0.2957 | 0.3332 | |
| | Present | 0.4916 | 0.5285 | 0.2957 | 0.3245 | 0.1750 |
| | Fasshauer | 0.4986 | 0.5360 | 0.2982 | 0.3499 | 0.1168 |
| | Franke | 0.5222 | 0.5629 | 0.3082 | 0.8994 | 0.0620 |
| | Hardy | 0.5254 | 0.5668 | 0.3100 | 1.0642 | 0.0584 |
| | Rippa | 0.5158 | 0.5541 | 0.3055 | 0.2318 | 0.0723 |
| 100 | FSDT exact | 0.4337 | 0.5382 | 0.2705 | 0.3390 | |
| | Present | 0.4611 | 0.5674 | 0.2800 | 0.4458 | 0.1950 |
| | Fasshauer | 0.6032 | 0.7191 | 0.3247 | 0.7997 | 0.1168 |
| | Franke | 7.9090 | 8.8313 | 1.8805 | 9.5939 | 0.0620 |
| | Hardy | 37.8063 | 42.071 | 7.6575 | 42.9480 | 0.0584 |
| | Rippa | 0.5246 | 0.6348 | 0.3017 | 0.6270 | 0.1406 |
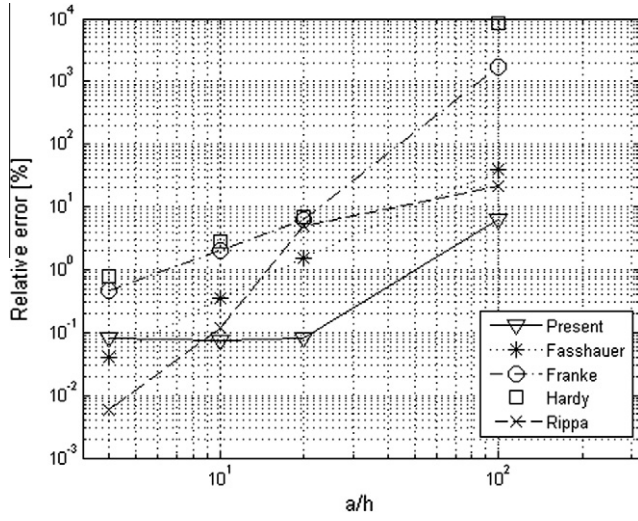
**Fig. 3.** Relative error on maximum displacement between the FSDT exact solution and the RBF solution with different shape parameters.
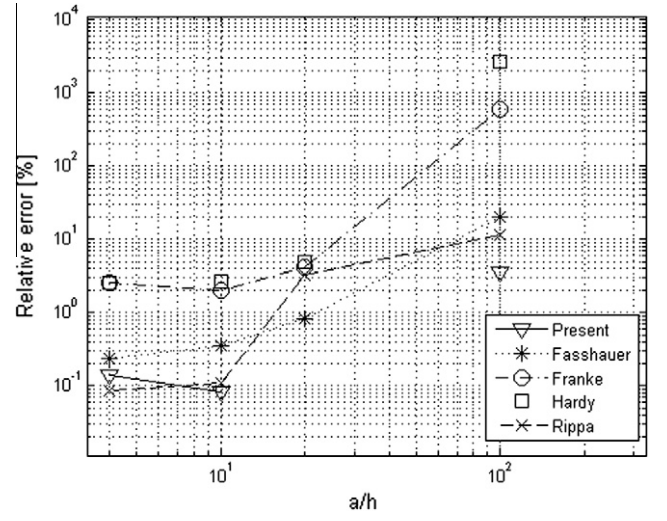


**Fig. 5.** Relative error on $\bar{\sigma}_{yy}$ between the FSDT exact solution and the RBF solution with different shape parameters.
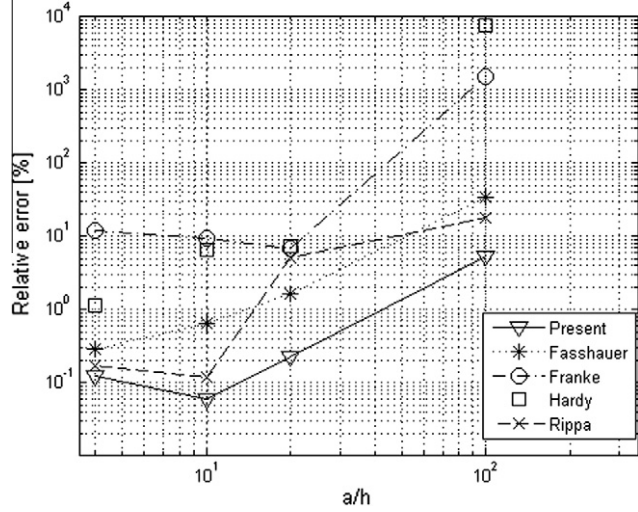


**Fig. 4.** Relative error on $\bar{\sigma}_{bixx}$ between the FSDT exact solution and the RBF solution with different shape parameters.
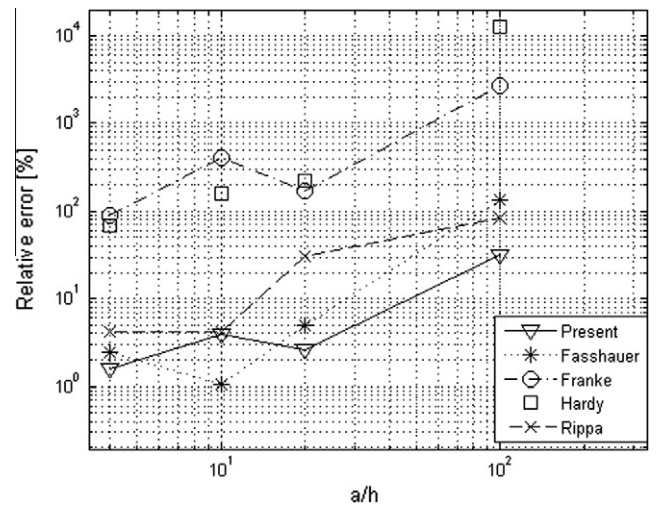


**Fig. 6.** Relative error on $\bar{\tau}_{xz}$ between the FSDT exact solution and the RBF solution with different shape parameters.

## 3. Static analysis of composite and sandwich plates using a Meshless solution approach

The First-order Shear Deformation Theory (FSDT) [14] is here briefly summarized as it will be used, coupled with the unsymmetric radial basis functions collocation method and the novel shape parameter selection procedure, for the analysis of multilayered composite and sandwich plates subjected to static loads.

### 3.1. FSDT basic equations

The FSDT displacement field is

$$\begin{cases} u(x,y,z) = u_0(x,y) + \phi_x(x,y)z \\ v(x,y,z) = v_0(x,y) + \phi_y(x,y)z \\ w(x,y,z) = w_0(x,y) \end{cases} \tag{10}$$

where $x$, $y$ and $z$ are the coordinates of a Cartesian orthogonal system ($z$ is the plate thickness coordinate while the $x-y$ plane corresponds to the plate reference surface); $u_0$, $v_0$ and $w_0$ are the displacements of a point on the reference surface, and $\phi_x$ and $\phi_y$

**Table 4**
Mechanical properties of the core.

| $E_1$ | $G_{12}$ | $v_{12}$ | $G_{13}$ | $G_{23}$ |
|---|---|---|---|---|
| 1.90 $E_2$ | 0.56 $E_2$ | 0.44 | 0.33 $E_2$ | 0.56 $E_2$ |

are the rotations of the transverse normal about the positive $y$-axis and negative $x$-axis, respectively. The equilibrium equations of the plate subjected to a transverse distributed load $\bar{q}(x,y)$ are

$$\begin{cases} N_{x,x} + N_{xy,y} = 0 \\ N_{y,y} + N_{xy,x} = 0 \\ Q_{x,x} + Q_{y,y} + \bar{q}(x,y) = 0 \\ M_{x,x} + M_{xy,y} - Q_x = 0 \\ M_{y,y} + M_{xy,x} - Q_y = 0 \end{cases} \tag{11}$$

where $N_x$, $N_{xy}$ and $N_y$ are the in-plane forces, $Q_x$ and $Q_y$ the shear forces, $M_x$, $M_{xy}$ and $M_y$ the bending moments. The constitutive

**Table 5**
Results for a simply supported sandwich plate subjected to a uniform pressure, $a/h = 10$, $R = 5$.

| Method | $f_1 \sigma_{xx}(\frac{a}{2},\frac{a}{2},-\frac{h}{2})$ | $f_1 \sigma_{yy}(\frac{a}{2},\frac{a}{2},-\frac{h}{2})$ | $f_1 \tau_{xz}(0,\frac{a}{2},0)$ | $f_2 w_{max}$ | $c_{opt}$ |
|---|---|---|---|---|---|
| FSDT exact | 59.06 | 38.00 | 4.42 | 258.30 | |
| Present (15 × 15 r) | 58.81 | 37.82 | 3.87 | 256.96 | 0.100 |
| Ferreira (15 × 15 r) [5] | 58.72 | 37.64 | 3.85 | 257.38 | – |
| Present (21 × 21 r) | 58.98 | 37.96 | 4.11 | 258.05 | 0.075 |
| Ferreira (21 × 21 r) [5] | 59.02 | 38.00 | 4.02 | 258.80 | – |
| Present (15 × 15 ir) | 59.44 | 38.41 | 3.87 | 260.23 | 0.090 |
| Present (15 × 15 ir2) | 59.09 | 37.94 | 3.66 | 256.88 | 0.090 |
| Present (21 × 21 ir) | 58.89 | 37.93 | 4.62 | 258.12 | 0.130 |
| Present (21 × 21 ir2) | 58.81 | 37.91 | 4.03 | 257.29 | 0.110 |

**Table 6**
Results for a simply supported sandwich plate subjected to a uniform pressure, $a/h = 10$, $R = 10$.

| Method | $f_1 \sigma_{xx}(\frac{a}{2},\frac{a}{2},-\frac{h}{2})$ | $f_1 \sigma_{yy}(\frac{a}{2},\frac{a}{2},-\frac{h}{2})$ | $f_1 \tau_{xz}(0,\frac{a}{2},0)$ | $f_2 w_{max}$ | $c_{opt}$ |
|---|---|---|---|---|---|
| FSDT exact | 63.04 | 42.71 | 4.16 | 158.74 | |
| Present (15 × 15 r) | 62.97 | 42.66 | 3.70 | 158.20 | 0.070 |
| Ferreira (15 × 15 r) [5] | 62.72 | 42.56 | 3.60 | 158.55 | – |
| Present (21 × 21 r) | 63.16 | 42.79 | 4.07 | 159.02 | 0.050 |
| Ferreira (21 × 21 r) [5] | 63.03 | 42.75 | 3.76 | 159.34 | – |
| Present (15 × 15 ir) | 63.92 | 43.18 | 3.74 | 160.86 | 0.110 |
| Present (15 × 15 ir2) | 63.00 | 42.56 | 3.46 | 157.36 | 0.070 |
| Present (21 × 21 ir) | 60.82 | 42.16 | 3.13 | 157.53 | 0.130 |
| Present (21 × 21 ir2) | 63.37 | 42.59 | 3.86 | 158.44 | 0.050 |

**Table 7**
Results for a simply supported sandwich plate subjected to a uniform pressure, $a/h = 10$, $R = 15$.

| Method | $f_1 \sigma_{xx}(\frac{a}{2},\frac{a}{2},-\frac{h}{2})$ | $f_1 \sigma_{yy}(\frac{a}{2},\frac{a}{2},-\frac{h}{2})$ | $f_1 \tau_{xz}(0,\frac{a}{2},0)$ | $f_2 w_{max}$ | $c_{opt}$ |
|---|---|---|---|---|---|
| FSDT exact | 63.52 | 45.18 | 4.05 | 121.17 | |
| Present (15 × 15 r) | 63.25 | 45.02 | 3.57 | 120.46 | 0.070 |
| Ferreira (15 × 15 r) [5] | 63.21 | 45.05 | 3.47 | 121.18 | – |
| Present (21 × 21 r) | 63.55 | 45.21 | 3.93 | 121.25 | 0.050 |
| Ferreira (21 × 21 r) [5] | 63.55 | 45.25 | 3.63 | 121.74 | - |
| Present (15 × 15 ir) | 55.40 | 39.71 | 2.38 | 106.04 | 0.050 |
| Present (15 × 15 ir2) | 62.86 | 44.83 | 3.50 | 120.05 | 0.100 |
| Present (21 × 21 ir) | 63.96 | 45.48 | 4.13 | 121.54 | 0.130 |
| Present (21 × 21 ir2) | 63.37 | 45.18 | 3.72 | 121.05 | 0.070 |
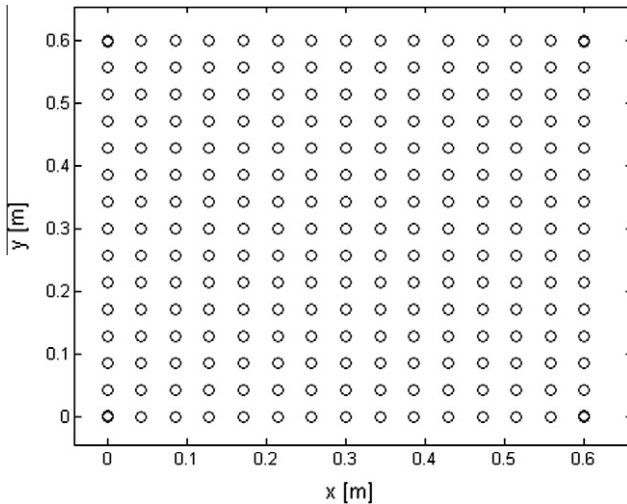


**Fig. 7.** Regular grid.
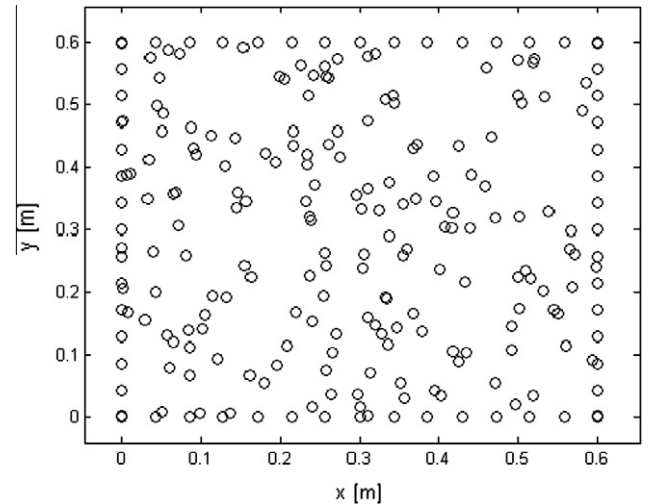


**Fig. 8.** Irregular grid (ir).

equations relating the resultant forces and moments to the strain measures are

$$\left\{\begin{array}{c} N_x \\ N_y \\ N_{xy} \end{array}\right\} = [A]\left\{\begin{array}{c} u_{0,x} \\ v_{0,y} \\ u_{0,y}+v_{0,x} \end{array}\right\} + [B]\left\{\begin{array}{c} \phi_{x,x} \\ \phi_{y,y} \\ \phi_{x,y}+\phi_{y,x} \end{array}\right\} \qquad (12)$$

$$\left\{\begin{array}{c} M_x \\ M_y \\ M_{xy} \end{array}\right\} = [B]\left\{\begin{array}{c} u_{0,x} \\ v_{0,y} \\ u_{0,y}+v_{0,x} \end{array}\right\} + [D]\left\{\begin{array}{c} \phi_{x,x} \\ \phi_{y,y} \\ \phi_{x,y}+\phi_{y,x} \end{array}\right\} \qquad (13)$$

$$\left\{\begin{array}{c} Q_x \\ Q_y \end{array}\right\} = k[A_T]\left\{\begin{array}{c} \phi_x + w_{,x} \\ \phi_y + w_{,y} \end{array}\right\} \qquad (14)$$

where $[A]$, $[B]$, $[D]$ and $[A_T]$ are the membrane, coupling, bending and transverse shear stiffness matrices [14], $k$ being the transverse shear correction factor. Several methods have been proposed for calculating the shear correction factors for multilayered composite [15] and sandwich [16] plates.

The equilibrium equations written in terms of kinematic unknowns may be obtained substituting the constitutive Eqs. (12)–(14) into Eq. (11). For the case of a symmetric cross-ply laminate, the equations governing the transverse behavior are uncoupled from those governing the in-plane behavior and read as follows

$$\begin{cases} D_{11}\frac{\partial^2 \phi_x}{\partial x^2} + D_{66}\frac{\partial^2 \phi_x}{\partial y^2} + (D_{12}+D_{66})\frac{\partial^2 \phi_y}{\partial x \partial y} - kA_{44}\left(\phi_x + \frac{\partial w}{\partial x}\right) = 0 \\ D_{22}\frac{\partial^2 \phi_y}{\partial y^2} + D_{66}\frac{\partial^2 \phi_y}{\partial x^2} + (D_{12}+D_{66})\frac{\partial^2 \phi_x}{\partial x \partial y} - kA_{55}\left(\phi_y + \frac{\partial w}{\partial y}\right) = 0 \\ kA_{44}\left(\frac{\partial \phi_x}{\partial x} + \frac{\partial^2 w}{\partial x^2}\right) + kA_{55}\left(\frac{\partial \phi_y}{\partial y} + \frac{\partial^2 w}{\partial y^2}\right) + q(x,y) = 0 \end{cases} \qquad (15)$$

### 3.2. Multiquadratic interpolation of the FSDT differential governing equations

Let us now apply the unsymmetrical radial basis function collocation method and the FSDT to the static analysis of a symmetric rectangular panel (dimensions $a \times b \times h$). The first step is to distribute $N$ nodes on the plate domain: the nodes inside the plate domain are numbered with $j = 1, \ldots, N_I$ while the ones placed on the boundary with $j = N_I + 1, \ldots, N_I + N_B = N$. The kinematic unknowns may be then written as

$$\left\{\begin{array}{c} w \\ \phi_x \\ \phi_y \end{array}\right\} = \sum_{i=1}^{N}\left\{\begin{array}{c} \alpha_i \\ \beta_i \\ \gamma_i \end{array}\right\}\phi_i(\boldsymbol{x}) \qquad (16)$$

where $\phi_i(\boldsymbol{x})$ represents the $i$th radial basis function (Eq. (4)) and $(\alpha_i, \beta_i, \gamma_i)$ are the $i$th kinematic unknown coefficients of the approximation. Substitution of Eq. (16) into Eq. (15) is done for the $N_I$ nodes inside the plate domain ($j = 1, \ldots, N_I$)

$$D_{11}\sum_{i=1}^{N}\beta_i\phi_{i,xx}(\boldsymbol{x}_j) + D_{66}\sum_{i=1}^{N}\beta_i\phi_{i,yy}(\boldsymbol{x}_j) + (D_{12}+D_{66})$$
$$\times \sum_{i=1}^{N}\gamma_i\phi_{i,xy}(\boldsymbol{x}_j) - kA_{44}\left(\sum_{i=1}^{N}\beta_i\phi_i(\boldsymbol{x}_j) + \sum_{i=1}^{N}\alpha_i\phi_{i,x}(\boldsymbol{x}_j)\right) = 0 \qquad (17)$$

$$D_{22}\sum_{i=1}^{N}\gamma_i\phi_{i,yy}(\boldsymbol{x}_j) + D_{66}\sum_{i=1}^{N}\gamma_i\phi_{i,xx}(\boldsymbol{x}_j) + (D_{12}+D_{66})$$
$$\times \sum_{i=1}^{N}\beta_i\phi_{i,xy}(\boldsymbol{x}_j) - kA_{55}\left(\sum_{i=1}^{N}\gamma_i\phi_i(\boldsymbol{x}_j) + \sum_{i=1}^{N}\alpha_i\phi_{i,y}(\boldsymbol{x}_j)\right) = 0 \qquad (18)$$
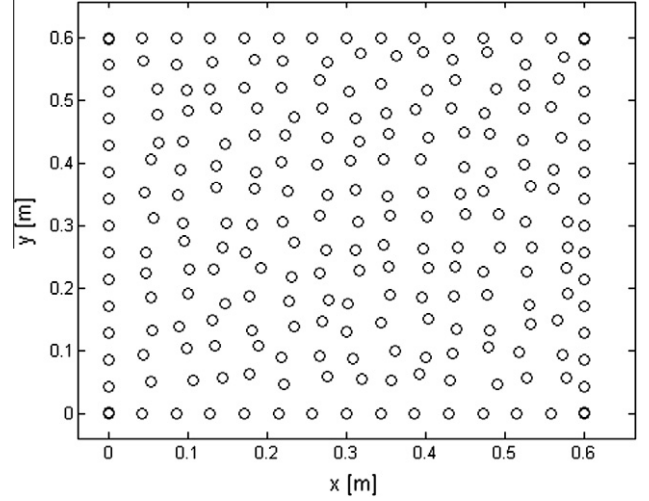
Fig. 9. Irregular grid (ir2).

$$kA_{44}\left(\sum_{i=1}^{N}\beta_i\phi_{i,x}(\boldsymbol{x}_j) + \sum_{i=1}^{N}\alpha_i\phi_{i,xx}(\boldsymbol{x}_j)\right)$$
$$+ kA_{55}\left(\sum_{i=1}^{N}\gamma_i\phi_{i,y}(\boldsymbol{x}_j) + \sum_{i=1}^{N}\alpha_i\phi_{i,yy}(\boldsymbol{x}_j)\right) + q(x_j,y_j) = 0 \qquad (19)$$

Boundary conditions are satisfied on the $N_B$ nodes located on the plate edges. For a plate simply supported on all four edges, the boundary conditions are

$$x = 0, a \rightarrow \begin{cases} w = 0 \\ M_x = 0 \\ \phi_y = 0 \end{cases} \quad y = 0, \quad b \rightarrow \begin{cases} w = 0 \\ M_y = 0 \\ \phi_x = 0 \end{cases} \qquad (20)$$

while, if the plate is fully clamped, the boundary conditions are

$$x = 0,\ a;\ y = 0,\ b \rightarrow \begin{cases} w = 0 \\ \phi_x = 0 \\ \phi_y = 0 \end{cases} \qquad (21)$$

For example, the boundary condition on the bending moments (20) will be written as follows when using the approximation (16)
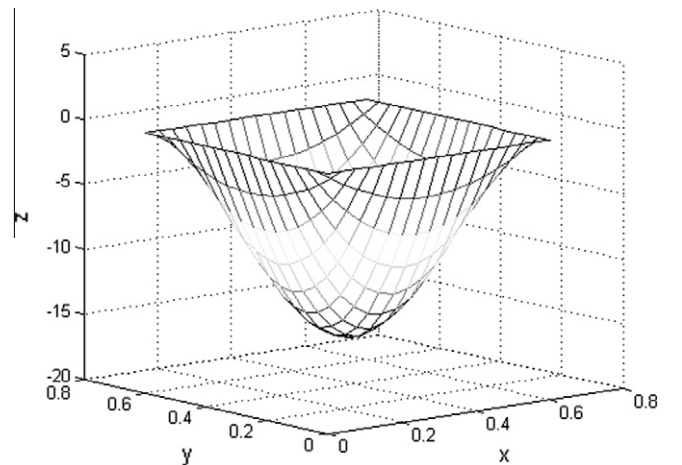
Fig. 10. Deformation of simply supported sandwich plate subjected to uniform pressure ($R = 5$).

**Table 8**
Results for a sandwich plate fully clamped subjected to uniform pressure, $a/h = 10$.

| Method | $f_1\sigma_{xx}(\frac{a}{2},\frac{a}{2},-\frac{h}{2})$ | $f_1\sigma_{yy}(\frac{a}{2},\frac{a}{2},-\frac{h}{2})$ | $f_1\tau_{xz}(0,\frac{a}{2},0)$ | $f_2 w_{max}$ | $c_{opt}$ |
|---|---|---|---|---|---|
| **$R = 5$** | | | | | |
| FSDT | 27.12 | 20.19 | 5.01 | 114.54 | |
| Present ($15 \times 15$ r) | 27.31 | 20.35 | 3.11 | 113.29 | 0.19 |
| Present ($21 \times 21$ r) | 27.43 | 20.42 | 3.46 | 113.74 | 0.14 |
| **$R = 10$** | | | | | |
| FSDT | 28.44 | 23.75 | 4.42 | 81.71 | |
| Present ($15 \times 15$ r) | 28.72 | 23.94 | 3.00 | 79.59 | 0.20 |
| Present ($21 \times 21$ r) | 28.82 | 24.01 | 3.14 | 79.82 | 0.14 |
| **$R = 15$** | | | | | |
| FSDT | 28.58 | 25.90 | 4.11 | 68.53 | |
| Present ($15 \times 15$ r) | 28.73 | 25.90 | 2.85 | 66.36 | 0.20 |
| Present ($21 \times 21$ r) | 28.84 | 25.98 | 2.97 | 66.51 | 0.14 |

$$M_x = D_{11}\sum_{i=1}^{N}\beta_i\phi_{i,x}(\boldsymbol{x}_j) + D_{12}\sum_{i=1}^{N}\gamma_i\phi_{i,y}(\boldsymbol{x}_j) = 0 \qquad (22)$$

$$j = N_I + 1, \ldots, N_J \quad \text{and} \quad j = N_J + 1, \ldots, N_L$$

$$M_y = D_{12}\sum_{i=1}^{N}\beta_i\phi_{i,x}(\boldsymbol{x}_k) + D_{22}\sum_{i=1}^{N}\gamma_i\phi_{i,y}(\boldsymbol{x}_k) = 0$$

$$k = N_L + 1, \ldots, N_M \quad \text{and} \quad k = N_M + 1, \ldots, N_N = N$$

where nodes numbered from $N_I + 1$ to $N_J$ and from $N_J + 1$ to $N_L$ are those placed on the boundary $x = 0$ and $x = a$, respectively. In a similar manner, nodes numbered from $N_L + 1$ to $N_M$ and from $N_M + 1$ to $N_N$, are those placed on the edge with $y = 0$ and $y = b$, respectively.

Considering the $3N_I$ equilibrium Eqs. (17)–(19) together with the boundary conditions based on Eq. (20) or (21), a linear system in terms of the unknown coefficients ($\alpha_i, \beta_i, \gamma_i$) is obtained.

## 4. Numerical results

In order to demonstrate the accuracy of the proposed approach for calculating the shape parameter $c$, numerical results pertaining elasto-static deformation of composite and sandwich plates are presented and compared with those obtained with different choices of the shape parameter and with analytical FSDT solutions.

### 4.1. Laminated composite plate subjected to a sinusoidal pressure

A cross-ply and symmetric composite plate, simply supported on all the edges and subjected to a bi-sinusoidal pressure

$$p(x,y) = P_0 \sin\left(\frac{\pi x}{a}\right)\sin\left(\frac{\pi x}{b}\right)$$

is considered. The layers have the same thickness and the stacking sequence is (0°/90°/90°/0°). Material mechanical properties of the unidirectional lamina are reported in non-dimensional form in Table 2.

Analyses will be conducted using $k = 5/6$, although authors are conscious that this value could be not the best choice for this laminate. Because the purpose of the paper is to assess the accuracy and reliability of the algorithm for the selection of parameter $c$, the use of a not suitable shear correction factor is not an issue, provided that comparisons with analytical solution are made under the same conditions, in particular with the same $k$. Readers which want to estimate a more adequate shear correction factor, could refer to [15].

Numerical results are obtained using a $17 \times 17$ regular grid ($N = 17$ r), where "r" stands for regular, and different aspect ratios $a/h$.

Table 3 shows the results obtained using the present approach (FSDT solved with the unsymmetric radial basis functions colloca-

tion method and the novel shape parameter selection) and the exact FSDT solution, all estimated with a shear correction factor $k = 5/6$. Furthermore, Table 3 compares solutions obtained using the unsymmetric radial basis functions collocation method and the shape parameter estimated by means of the models shown in Section 2.1. The transverse shear stresses have been estimated integrating the equilibrium equations. Stresses and displacements are given in the following non-dimensional form

$$\bar{w} = \frac{10^2 w_{max} h^3 E_T}{P_0 a^4} \qquad \bar{\sigma}_{xx} = \frac{\sigma_{xx}(a/2, a/2, h/2)h^2}{P_0 a^2}$$

$$\bar{\sigma}_{yy} = \frac{\sigma_{yy}(a/2, a/2, h/4)h^2}{P_0 a^2} \qquad \bar{\tau}_{xz} = \frac{\tau_{xz}(0, a/2, 0)h}{P_0 a}$$

In order to make the comparison easier, in Fig. 3 the relative error between the maximum displacement estimated by means the FSDT exact solution and the others collected in Table 3 is represented. The same comparison, now on the stresses, is shown in Figs. 4–6.

Generally speaking, results obtained with the present algorithm for the selection of the shape parameter are better than those estimated with other models, in particular for thin plates. As for the other models, these could ensure, sometimes, accurate results; the best appears to be the Fasshauer's one. As stated in [4], the Rippa's algorithm is applied to a user-defined interval, which has to be carefully chosen. It has been observed by Rippa [12] that the error presents two distinct behaviors: the former, more stable, is confined in a small interval of $c$; the latter could be very erratic. Thus it is important to select an interval inside the stable region. This could be achieved selecting a large interval at the first time and then focusing on a smaller one. The interval that has been used to obtain the results presented in Table 3 is [0.01, 0.2].

### 4.2. Sandwich plate subjected to a uniform pressure

In order to investigate the effect of the stacking sequence and the regularity of the grid on the shape parameter selection, we have considered a sandwich square plate, loaded with a transverse uniform unit pressure.[2] The core is assumed to be orthotropic and its mechanical properties are collected in Table 4.

The mechanical properties of the face are those of the core multiplied by $R$ (except for the Poisson ratio). The sandwich plate has an aspect ratio $a/h = 10$ while the thickness of the core is eight times that of each skin, $h_c/h_f = 8$.

---

[2] Authors are aware that classical FSDT model is not well suited for the analysis of sandwich plates but they have used this approach in order to compare present results with those quoted in Ref. [5].
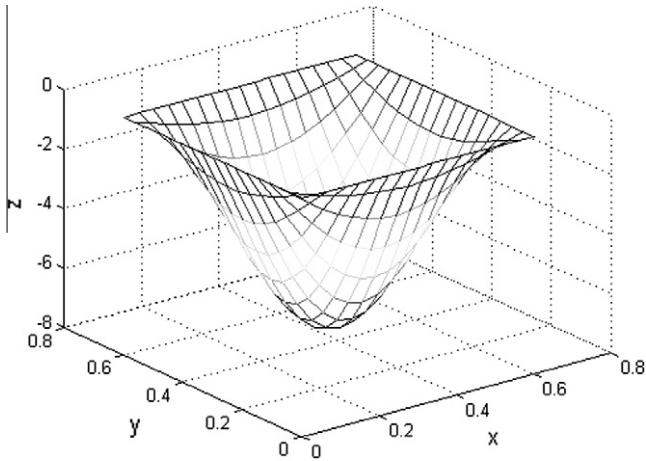
**Fig. 11.** Deformed shape of a fully clamped sandwich plate subjected to a uniform pressure.

Results from the present model are compared with FSDT exact solutions and those obtained by Ferreira et al. [5]. Tables 5–7 compare results in terms of transverse displacements, normal and shear stresses. Transverse displacement and stresses are normalized through factors

$$f_2 = \frac{0.999781}{hq}; \quad f_1 = \frac{1}{q}$$

Also in these cases, transverse shear stresses are computed by integration of the equilibrium equations. In order to compare the results, the same shear correction factor is used as estimated by the procedure given in [5,15].

Two grids are considered: a $15 \times 15$ and a $21 \times 21$ regular grid (Fig. 7). In order to evaluate the performance of the Meshless method with the present algorithm for the selection of $c$, also $15 \times 15$ and $21 \times 21$ irregular grids have been used. The irregular grids are two: the first (Fig. 8), denoted by "ir", is generated by means the MATLAB® command *rand*, while the second, denoted by "ir2", derives from a regular one that has been perturbed (nodes are shifted both in $x$ and $y$ direction of a random quantity that is lower than the distance between the nodes in the regular grid). We thus perturb the regular grid in order to obtain an irregular one like that in Fig. 9.

The use of an irregular grid (ir) leads sometimes to relevant errors that should be due, according to the authors, to the generation of a grid with two or more nodes so close that are almost coincident. This causes an ill-conditioning of the problem with an obvious loss of accuracy. In fact, taking into consideration the results in Tables 5–7, those related to the irregular grid (ir2) are more stable than ones estimated with the fully irregular grid (ir).

In Fig. 10 a typical deformation of the plate is illustrated. Deformed shape is quite smooth and represents quite well the expected deformation.

In order to show the robustness of the approach, results for a fully clamped plate are given in Table 8.

Also in this case, the results are obtained with a value of the shape parameter estimated by the algorithm presented in this paper. In Fig. 11 a typical deformation of a fully clamped plate is illustrated.

## 5. Conclusions

In this paper we focused on Radial Basis Function Collocation Methods for solving the equations governing the static behavior of sandwich and multilayered composite structures. In particular we have taken into consideration the Unsymmetric RBF Collocation Method using the MultiQuadratic (MQ) functions. The MQ functions introduce a shape parameter, $c$, that affects the accuracy of the solution leading sometimes to ill-conditioning of the problem. This requires finding an optimal value of the shape parameter in order to obtain accurate solutions.

After a review of several methods by which estimating the optimal $c$, we have presented a new approach based on a convergence analysis. Some of the existing methods are related only with the number of nodes and the distances between them, thus the value of the shape parameter does not depend on the distribution of nodes, condition number of the matrix, computer precision and interpolation function. Our method is based on a convergence analysis and thus it is able to account for all the key effects.

In order to assess the accuracy of the proposed new approach, multilayered composite and sandwich plates subjected to various loads and with different boundary conditions are analyzed using the First-order Shear Deformation Theory and the unsymmetric RBF collocation method with different choices of the optimal shape parameter. As for the analysis of statically loaded composite plates, the present method ensures relative errors on the maximum displacement, on $\bar{\sigma}_{xx}$, and on $\bar{\sigma}_{yy}$ lower than 1%, unlike other methods, until the aspect ratio $a/h$ is less than 20. For thinner plates, lower accuracy is experienceded but the present method works better than the other ones. When analyzing sandwich plates, solutions have been obtained with different types of grid (regular, irregular and perturbed regular) and with different boundary conditions. The novel algorithm shows its efficiency both with regular and irregular grid. Since the shape parameter computed by means of the present algorithm is different depending a regular grid or an irregular one is used, then it is assessed that the shape parameter is affected also by the distribution of nodes.

As it is possible to catch pointing out Table 8, the present method works very well also with boundary conditions different from the classical simply support.

Future enhancements of this activity will enclose the application of the present new method for optimal shape parameter choice to the analysis of multilayered composite and sandwich plates with the Refined Zigzag Theory [17].

## References

[1] Liu GR. Mesh free methods: moving beyond the finite element method. CRC Press; 2003.

[2] Liu GR, Gu YT. An Introduction to Meshfree methods and their programming. Springer; 2005.

[3] Power H, Barraco V. A comparison analysis between unsymmetric and symmetric radial basis function collocation methods for the numerical solution of partial differential equations. Comput Math Appl 2002;43:551–83.

[4] Roque CMC, Ferreira AJM. Numerical experiments on optimal shape parameters for radial basis functions. Numerical methods for partial differential equations, vol. 26 (3). Wiley; 2010. p. 675–89.

[5] Ferreira AJM. A formulation of the multiquadratic radial basis function method for the analysis of laminated composite plates. Compos Struct 2003;59:385–92.

[6] Huang CS, Lee C-F, Cheng AH-D. Error estimate, optimal shape factor, and high precision computation of multiquadratic collocation method. Eng Anal Bound Elem 2007;31:614–23.

[7] Hardy RL. Multiquadratic equations for topography and other irregular surfaces. J Geophys Res 1971;176:1905–15.

[8] Franke R. Scattered data interpolation tests of some methods. Math Comput 1982;38:181–200.

[9] Fasshauer GE. Newton iteration with multiquadratics for the solution of nonlinear pdes. Comput Math Appl 2002;43:4234–438.

[10] Ferreira AJM, C Roque CM, Jorge RMN. Natural frequencies of FSDT cross-ply composite shells by multiquadratics. Compos Struct 2007;77:296–305.

[11] Ferreira AJM, Fasshauer GE. Analysis of natural frequencies of composite plates by an RBF – pseudospectral method. Compos Struct 2007;79:202–10.

[12] Rippa S. An algorithm for selecting a good value for the parameter c in radial basis function interpolation. Adv Comput Math 1999;11:193–210.

[13] Ferreira AJM, Fasshauer GE, Batra RC, D Rodrigues J. Static deformations and vibration analysis of composite and sandwich plates using a layerwise theory and RBF-PS discretizations with optimal shape parameter. Compos Struct 2008;86:328–43.

[14] Reddy JN. Mechanics of laminated composite plates and shells. CRC Press LLC; 2004.

[15] Vlachoutsis S. Shear correction factors for plates and shells. Int J Numer Methods Eng 1992;33:1537–52.

[16] Birman V, Bert CW. On the choice of the shear correction factor in sandwich structures. J Sandwich Struct Mater 2002;4:83–95.

[17] Tessler A, Di Sciuva M, Gherlone M. Refined zigzag theory for laminated composite and sandwich plates. NASA/TP-2009-215561.